Seasonal Variation of Land-Atmosphere Coupling Strength over the West African Monsoon Region in an Atmospheric General Circulation Model

Tomohito J. Yamada[1], Shinjiro Kanae[2], Taikan Oki[3], and Randal D. Koster[4]

[1]Faculty of Engineering, Hokkaido University, Kita-13 Nishi-8, Kita-ku, Sapporo, Hokkaido 060-8628, Japan

[2]Department of Mechanical and Environmental Informatics, Tokyo Institute of Technology, Tokyo, 152-8552, Japan

[3]Institute of Industrial Science, The University of Tokyo, Tokyo, 153-8505, Japan

[4]Global Modeling and Assimilation Office, NASA Goddard Space Flight Center, MD, 27700, USA

Corresponding author: Tomohito Yamada

Faculty of Engineering, Hokkaido University, Kita-13 Nishi-8, Kita-ku, Sapporo, Hokkaido 060-8628, Japan

Email: tomohito@eng.hokudai.ac.jp

Abstract

The seasonal variation of land-atmosphere coupling strength has been examined using an extended series of atmospheric general circulation model (AGCM) simulations. In the western Sahel of Africa, strong coupling strength for precipitation is found in April and May, just prior to and at the beginning of the monsoon season. At this time, heat and water fluxes from the surface are strongly controlled by land conditions, and unstable conditions in the lower level of the troposphere, as induced by local land state, allow the surface fluxes to influence the variability of convective precipitation – and thus the timing of monsoon onset.

Keywords

Land-Atmosphere Interactions, Coupling Strength, West African Monsoon, Soil Moisture, Evapotranspiration, AGCMs

1. Introduction

Given that soil moisture anomalies may persist for weeks to months, and given that soil moisture anomalies affect the surface energy budget and thus perhaps affect air temperature and the generation of precipitation, knowledge of sub-surface soil moisture conditions at the start of a seasonal or subseasonal forecast can potentially increase the skill of the forecast (Koster et al. 2010). In effect, quantifying the impact of soil moisture on the evolution of weather is a two-pronged problem: an "initialization" problem associated with soil moisture memory and a "boundary condition" problem associated with atmospheric response to surface anomalies. Soil moisture memory has been investigated extensively both in observational and numerical model-based studies (e.g., Vinnikov and Yeserkepova 1991, Entin et al. 2000, Koster and Suarez 2001, Shinoda and Yamaguchi 2003, Seneviratne et al. 2006). The additional problem of the potential impact of soil moisture on the seasonal evolution of meteorological states has typically been examined with atmospheric general circulation models (AGCMs) (e.g., Shukla and Mintz 1982, Fennessy and Shukla 1999, Douville and Chauvin 2000, Koster et al. 2000). Kanae et al. (2006) investigated the impact of realistic soil moisture variations on precipitation variability. The realistic soil moisture dataset was produced by Hirabayashi et al. (2005) using observations-based precipitation and re-analyzed atmospheric data.

The sensitivity of precipitation variability associated with land surface anomalies is termed the land-atmosphere coupling strength, and it can be quantified for AGCMs using highly controlled experiments. The Global Land–Atmosphere Coupling Experiment (GLACE) was an

1 international project in which a dozen modeling groups performed such experiments and
2 thereby quantified the land–atmosphere coupling strength for boreal summer. The GLACE
3 study in particular quantified the ability of subsurface soil moisture variability to affect
4 precipitation variability (6 day-averages were examined over a 3 month period). GLACE
5 showed that coupling strength is largely model-dependent, reflecting, for example,
6 model-specific treatments of subsurface hydrology, canopy evapotranspiration, boundary layer
7 turbulence, and moist convection. Even so, the multi-model results from the 12 AGCMs reveal
8 consensus regions of strong coupling strength; the so-called "hot spots" found in central North
9 America and other transition zones between wet and dry climates (Koster et al. 2004, 2006).
10 Guo et al. (2006) suggested that the ability of soil moisture to affect precipitation should be
11 examined in two stages: the ability of the soil moisture to affect evaporation, and the ability of
12 evaporation to affect precipitation. Especially strong coupling occurs when the evaporation rate
13 varies strongly with soil moisture.
14
15 The present study establishes the seasonality of coupling strength between land surface states
16 and precipitation in the western Sahel, a region for which the land-sea temperature contrast may
17 influence the strength of monsoon activity (e.g., Folland and Palmer 1986, Webster et al. 1998,
18 Vizy and Cook 2000, Vizy and Cook 2002). Many papers have discussed the importance of
19 strong meridional soil moisture gradients for the evolution of the Sahelian monsoon, an implicit
20 indication that land-atmosphere coupling strength does play a role there (e.g., Cook 1999,
21 Sultan and Janicot 2003, Yamada et al. 2012). Koster et al. (2004), in the GLACE project,

showed that current AGCMs tend to show a strong coupling between subsurface moisture and precipitation in this particular region. The GLACE project, however, also found large inter-model differences in simulated coupling strength. Such inter-model variability is in fact mirrored in various other studies, with different models producing radically different hydro-meteorological fields over the Western Sahel region (e.g., Cook and Vizy 2006, Hourdin et al. 2010, Xue et al. 2010). This implies an important caveat for the present study, which by logistical necessity examines the coupling strength in the Western Sahel with a single model. The limitations of using a single model must be kept in mind when interpreting our results. Note, however, that the use of a single model also provides a distinct advantage; it provides the flexibility to delve more deeply into the physical mechanisms controlling land-atmosphere coupling.

Section 2 describes our study's methodology, and in section 3, the seasonality of land-atmosphere coupling strength is analyzed over the West African monsoon region. Section 4 summarizes the results.

2. Methodology

2.1 Model and data

The model used in this study was the Center for Climate System Research/National Institute for Environmental Studies (CCSR/NIES) AGCM version 5.6 (T42 horizontal resolution), which was developed and improved by the Center for Climate System Research, the University of

Tokyo, and the National Institute for Environmental Studies (Numaguti et al. 1997). CCSR/NIES AGCM uses the Arakawa and Schubert cumulus parameterization scheme (Arakawa and Schubert 1974) and Mellor and Yamada's turbulence closure model level 2 (Mellor and Yamada 1982). For the land-surface scheme, we adopted the Minimal Advanced Treatments of the Surface Interaction and RunOff (MATSIRO) model, designed to represent biospheric processes such as photosynthesis (Takata et al. 2003). The Atmospheric Model Inter-comparison Project 2 (AMIP2) monthly mean sea surface temperature (SST) data were used to represent conditions at the ocean boundary.

2.2 Experimental design

In the present study, we performed two ensembles of AGCM simulations, following the framework of GLACE. Both ensembles consisted of 16 members (defined by differing initial conditions), each covering the period 1 March 1994 to 30 June 1995. To make 16 sets of initial conditions, we repeated 1994 year runs 16 times (using AMIP SST) and stored instantaneous data at the beginning of March 1st for each run. The "W" ensemble consisted of standard AGCM simulations with full land-atmosphere coupling; the land and atmospheric model states were free to evolve together. In the "R" ensemble, on the other hand, the land states at every time step were prescribed to values produced in one of the simulations in the W ensemble. In other words, the atmosphere in every simulation in the R ensemble was subjected to the same time-varying land boundary conditions. (See Koster et al. 2006 for full details of the experimental design.) The MATSIRO land variables prescribed in the R ensemble were soil

moisture, soil temperature, soil ice, soil skin temperature, canopy temperature, canopy intercepted water, snow, snow temperature, and snow albedo.

The R ensemble includes the prescription of states (e.g., hourly temperature variations) that are not inherently predictable at weekly to monthly timescales. As a result, our results may have little practical relevance to operational prediction at these timescales. Even so, they provide a useful means of understanding connections in the climate system – how variability in all land states together influences variability in the overall system. Variability in the fast reservoirs (surface soil moisture and skin temperature), by the way, is of particular interest in the modern era because it is potentially retrievable via satellite remote sensing (e.g., Reichle et al. 2008).

We used the statistical index Ω to quantify the land-atmosphere coupling strength (Koster et al. 2002). Details of the mathematical structure and statistical characteristics of Ω are provided by Yamada et al. (2007). Ω is calculated from the number of ensemble members (m), the temporal variance of the ensemble mean time series ($\hat{\sigma}^2$), and the full sample variance (σ^2):

$$\Omega = \frac{m\hat{\sigma}^2 - \sigma^2}{(m-1)\sigma^2}. \qquad (1)$$

If each ensemble member produces exactly the same time series, then $\hat{\sigma}^2$ equals σ^2, and Ω becomes 1. However, if the time series of all ensemble members are completely unrelated, Ω

approximates 0.

Note that for the W ensemble, similarity in a quantity's time series across ensemble members can result only from the prescribed boundary conditions at the ocean, from the prescribed land surface vegetation properties, and from the prescribed incident radiation at the top of the atmosphere. For the R ensemble, the similarity can also stem from the prescribed land boundary conditions. The land impacts are thus isolated by taking the difference of $\Omega(R)$ and $\Omega(W)$. When $\Omega(R)-\Omega(W)$ (our measure of "coupling strength") goes to 1, the prescription of the land surface states dominates atmospheric variability. When this difference goes to zero, the land boundary has no impact on atmospheric variability.

3. Seasonal variation of land-atmosphere coupling strength: Impact of the African monsoon

3.1 Seasonality of land-atmosphere coupling strength for precipitation

Figures 1 and 2 show the geographical distributions of seasonal mean precipitation and wind vectors at the 850hPa level from observations (Figure 1) and from the ensemble mean states in the W experiment (Figure 2) for the periods March to May (MAM), June to August (JJA), September to November (SON), and December to February (DJF). The observations underlying Figure 1 come from the Global Soil Wetness Project 2 (GSWP2) for precipitation

(Dirmeyer et al. 2006) and from the 25-yr Japanese Reanalysis (JRA25) for wind (Onogi et al. 2007). Our GCM reproduces reasonably well the seasonal mean precipitation and wind fields, though the model does tend to overestimate precipitation, particularly over the western Sahel in MAM and JJA.

Figure 3 shows the geographical distributions of land-atmosphere coupling strength ($\Omega_P(R)-\Omega_P(W)$) for precipitation (P) for each of the four seasons. Note that while all simulations were global, only the highlighted western Sahel region is shown here. A $\Omega_P(R)-\Omega_P(W)$ difference of 0.06 represents a value significantly different from zero at the 95% confidence level, as established by Monte Carlo analysis.

In the western Sahel, a large coupling strength is found for MAM (Figure 3a) which corresponds to the pre-monsoon season. Over the same region, Dirmeyer et al. (2009) showed significant correlations between GSWP-2 multi model analysis estimates of daily evaporation and subsurface soil moisture. Van der Ent et al. (2010) also suggested that most of the precipitation is of terrestrial origin. In JJA, SON, and DJF, however, the coupling strength does not satisfy the 95% significance test in many parts of the western Sahel (Figure 3b-d). We investigate now whether the large coupling strength for MAM is a result of land surface properties controlling the onset date and strength of the monsoon.

3.2 Role of the evaporation signal

Figure 4-a shows the seasonal cycles of $\Omega_P(W)$ and $\Omega_P(R)$ (computed using a 15-day moving average window) for the western Sahel region. The difference between $\Omega_P(W)$ and $\Omega_P(R)$ is large from March to June, and thus this is the time of year when land-atmosphere coupling is important (in agreement with Figure 3). Figure 5 shows the precipitation time series in the western Sahel for the individual ensemble members (colored lines indicate the ensemble mean in each experiment). This figure indicates that the distinction between ensembles W and R appears to be related to monsoon onset – in ensemble W, the date of monsoon onset appears more variable, with a range of about a month. (We arbitrarily define the onset date as the time at which the 6-day average precipitation meets or exceeds 2mm/day.) The onset dates for the W experiment range from the end of March (Mar. 19-24) to the beginning of May (Apr. 30-May 5), whereas those for the R experiment range only from the middle of April (Apr. 12-17) to the beginning of May (Apr. 30-May 5). In contrast, the monsoon withdrawal date (defined as the time when the 6-day average precipitation becomes less than 2mm/day.) appears to be independent of land surface variability.

The monsoon is strongest in the western Sahel in July and August, and during these two months, the spread of precipitation among the ensemble members is large in both the W and R ensembles (Figure 5). The spread is apparently not reduced in the R ensemble presumably because in the W ensemble, the surface soil wetness does not vary much among the ensemble members (Figure 6), staying close to the limit imposed by the water capacity. During this period, forcing parameters (e.g., SST and solar radiation) would dominate the temporal

variability of surface water and heat fluxes. Similarly, during the monsoon withdrawal season (September to November), the spread of precipitation in the two ensembles is similar.

Figure 4-b shows the seasonal cycle of $\sigma_E(W)\left[\Omega_E(R)-\Omega_E(W)\right]$ for the western Sahel region, where $\sigma_E(W)$ is the standard deviation of evapotranspiration, E, in the W experiment (when E is aggregated to 6-day totals). Guo et al. (2006) showed evidence that coupling strength for precipitation is determined by the local value of $\sigma_E(W)\left[\Omega_E(R)-\Omega_E(W)\right]$, a diagnostic that reflects both the strength of the evaporation signal (a major conduit by which surface information is transmitted to the atmosphere) and its coherence between ensemble members. In Figure 4b, we see that $\sigma_E(W)\left[\Omega_E(R)-\Omega_E(W)\right]$ is indeed largest in the pre-monsoon season both in 1994 and 1995, which corresponds to the period of high land-atmosphere coupling strength in Fig. 4-a. This result supports those of Dirmeyer et al. (2009) and Van den Hurk and van Meijgaard (2010), who found a high correlation between soil moisture and evaporation in MAM over the western Sahel. A global analysis of the connections between $\sigma_E(W)\left[\Omega_E(R)-\Omega_E(W)\right]$ and $\Omega_P(R)-\Omega_P(W)$ in this model (not shown) suggests that the July and August values of $\sigma_E(W)\left[\Omega_E(R)-\Omega_E(W)\right]$ in Figure 4b are probably too small to have a significant impact on $\Omega_P(R)-\Omega_P(W)$ for two reasons i) σ_E is itself small, implying a weak evaporation signal, and (ii) the evaporation signal that does exist is not strongly similar amongst the members of the R ensemble.

All this taken together suggests a partial explanation for the strong control of land surface states

on the date of monsoon onset but not on the peak monsoon precipitation strength or on the date of monsoon withdrawal. Simply put, at the start of the monsoon season, soil moistures are low enough to allow land states to regulate evaporation (as evidenced by higher $\sigma_E(W)\left[\Omega_E(R)-\Omega_E(W)\right]$ values), with a corresponding impact on rainfall. Once the monsoon arrives and fully wets the soil, however, evaporation is controlled more by atmospheric demand than by land surface state variations, and the land states have a correspondingly smaller impact on the remainder of the monsoon's life cycle.

Our study shows that the land surface state has a significant impact on the timing of the monsoon onset. However, the land's impact might not be limited to the onset stage. In a different region, Kanae at al. (2001) used a fine resolution regional atmospheric model to show that deforestation can affect the date of monsoon withdrawal in South East Asia. By modifying albedo and roughness length, deforestation has a strong impact on evapotranspiration, particularly during the withdrawal period, for which the natural (unmodified) vegetation density would be largest due to continued growth through the rainy season. In effect, deforestation has the potential to influence strongly the land-atmosphere coupling strength during later stages of the monsoon by changing the nature of evaporation during these periods. More detailed analysis with a finer resolution AGCM than used in this study may provide us with the means to address this aspect of the problem.

3.3 Role of atmospheric boundary layer

In addition to examining evaporation behavior, it is instructive to examine the nature of the atmosphere over the monsoon's life cycle. Figure 7-b shows the bulk Richardson number (hereafter; Ri) in the lower level of the troposphere (925hPa). The large negative values of Ri during the monsoon onset season indicate strongly unstable conditions, with associated large values for the vertical diffusion coefficient. Figure 7-a shows the time series of precipitation separated into its convective (blue) and large-scale (green) components. Summing together the blue and green bars gives the total precipitation. (A caveat is appropriate here. While AGCMs do compute convective and large-scale precipitation separately, the convective component is largely parameterized given that the AGCMs cannot resolve individual convective cells. Convective precipitation in a given AGCM is thus strongly dependent on resolution and on the particular convective parameterization adopted.) Each precipitation component in the figure is averaged over the 16 ensemble members of the W experiment. Notice that most of the precipitation from March to June is convective precipitation, which is produced by one-dimensional (vertical) processes with triggers near the surface. Convection is more strongly associated with land-atmosphere coupling than is large scale precipitation, since the setting off of these triggers is largely a function of variations in the state of the planetary boundary layer, which itself is strongly controlled by variations in land surface fluxes. Together, these atmospheric diagnostics imply that rainfall is more likely to be affected by land surface anomalies during the onset of the monsoon season than later. As for the end of the monsoon season, the land-precipitation coupling strength becomes weaker due to a lack of soil moisture variability (as discussed before).

Figure 8 shows the time series of lifting condensation level (hereafter; LCL) for the 16 members of the W and R ensembles. LCL is the height at which an air parcel, adiabatically lifted, is first saturated. In the figure, the vertical axis denotes the height of the condensation level above the land surface. The LCL helps determine the potential for moist convection, and because the LCL is highly dependent on the surface temperature field, the prescription of land surface states could in fact be influencing monsoon onset in part through the surface temperature. The spread of the LCL among the members of the R ensemble is much smaller than that for the W ensemble in April and May (pre-monsoon season), implying a strong impact of the land surface during these months on the potential for convection.

The results in Figure 8 can be contrasted with those of Van den Hurk and van Meijhgaard (2010), who showed an insensitivity of LCL to soil moisture in MAM. These results are not inconsistent with those shown here when one considers that the present results may reflect the prescription of surface temperature in the R experiment rather than the prescription of soil moisture. Also potentially playing a role are differences in the time scales considered in the two studies (monthly vs. 6-day) and, of course, model-specific biases.

In September and October (the withdrawal season), the spread of the LCL members is small for both the W and R ensembles, again perhaps reflecting the fact that even though soil moisture is not prescribed in the W ensemble, the W ensemble members all show similarly very wet soil

moisture values following a full season of rainfall. Potential impacts of variations in land states on the LCL during the withdrawal season are thus reduced.

These issues are driven home further by Figure 6b, which shows a scatter diagram of 6-day averaged surface soil moisture of all W ensemble members against spread among the members in the target western Sahel region. Colors indicate values for each month from April to October. (There are 5 time periods in a month.) The withdrawal season clearly has a smaller spread among the ensemble members than the pre-monsoon season, with more of the circles located at higher soil moisture values. This is again consistent with the idea that in the later period, for the W experiment, the extensive rains act to (nearly) saturate the soil, so that the evaporation is mainly controlled by atmospheric forcing and not by variations in soil moisture, which are small in any case. Near-surface temperature and specific humidity also have a smaller spread in the withdrawal season (not shown).

4. Summary and Discussion

This study used the CCSR/NIES AGCM to show that in the Sahel, the strength of land-atmosphere coupling varies seasonally. The strongest coupling strength in the western Sahel occurs in the monsoon onset season; indeed, the timing of monsoon onset appears to be controlled by the prescription of the land surface states. During the monsoon onset season, evaporation is more strongly controlled by land states, and unstable conditions in the lower

level of the troposphere appear to allow surface heat and water fluxes to influence the atmosphere through the instigation of convective activity. Also, the prescribed surface temperatures help determine the height of the lifting condensation level; note that these temperatures, even if they were not explicitly prescribed, could still be strongly controlled by the prescribed soil moistures through the relationship between soil moisture and evaporative cooling (not examined here).

Our results disagree somewhat with those of Van den Hurk and van Meijgaard (2010), who showed a strong sensitivity of the regional recycling ratio to soil moisture anomaly in, for example, JJA; in effect, they show a significant impact of soil moisture on precipitation later in the monsoon season, whereas we show almost none during this period. A study of their Sahelian soil moistures (their Figure 5) suggests a possible explanation. In their model, soil moistures from June through August span the full range of possible soil moisture contents, whereas in ours, soil moisture throughout this period is much closer to its maximum value. In the absence of measurements, of course, the truth is unknown. The comparison with Van den Hurk and van Meijgaard (2010) points out clearly the importance of considering model dependence in this type of study. Our study, while complete and self-consistent, is nevertheless subject, as all such studies are, to the impacts of model bias.

The land's impact is relatively small during the peak and cessation of the African monsoon. We note, however, that this is not a globally applicable result; in certain other regions, such as

central North America (results not shown), the timing of the cessation of the monsoon does, in fact, seem to be controlled in the AGCM in part by the specified land surface states.

In the broadest sense, our overall understanding of how variations in land surface state contribute to the variability of the Earth's climate system is still largely incomplete. The present study shows how carefully designed numerical experiments with an Earth system model can be used to further our understanding of land-climate interaction.

Acknowledgments.

This work was supported by the MEXT SOUSEI program (theme C-i-C), the Research Program on Climate Change Adaptation (RECCA/MEXT), the Science Technology Research Partnership for Sustainable Development (JST-JICA), and the Core Research for Evolutional Science and Technology program (CREST/JST). All computational resources were provided by the National Institute for Environmental Studies.

References

Arakawa, A. and Schubert, W. H., 1974. Interactions of cumulus cloud ensemble with the large-scale environment. Part I. *Journal of Atmospheric Sciences*, **31**, 671-701.

Cook, K. H.,1999. Generation of the African Easterly Jet and its role in determining West African precipitation. *Journal of Climate*, **12,** 1165-1184.

Cook, K. H., Vizy, E. K., 2006. Coupled Model Simulations of the West African Monsoon System: Twentieth- and Twenty-First-Century Simulations. *Journal of Climate*, **19**, 3682-3703.

Dirmeyer, P. A., Gau, X., Zhao, M., Guo, Z., Oki, T., and Hanasaki, N.,2006. GSWP-2: Multi Analysis and Implications for Our Perception of the Land Surface. *Bulletin of American Meteorological Society*, **87**, 1381-1397.

Dirmeyer, P. A., Schlosser, C. A., and Brubaker, K. L., 2009. Precipitation, Recycling, and Land Memory: An Integrated Analysis. *Journal of Hydrometeorology*, **10**, 278-288.

Douville, H. and Chauvin, F., 2000. Relevance of soil moisture for seasonal climate predictions: A preliminary study. *Climate Dyn*amics, **16,** 719–736.

Entin, J. K., Robock, A., Vinnikov, D. Y., Hollinger, S. E., Liu, S. and Namkhai, A., 2000. Temporal and spatial scales of observed soil moisture variations in the extratropics. *Journal of Geophysical Research*, **105**, 11,865-11,877.

Fennessy, M. J. and Shukla, J., 1999. Impact of initial soil wetness on seasonal atmospheric

prediction. *Journal of Climate*, **12**, 3167–3180.

Folland, G.K. and T. N. Palmer, 1986. Sahel rainfall and worldwide sea temperatures, 1901-85. Nature, **320**, 17, 602-607.

Guo, Z. and 24 co-authors, 2006. GLACE: The Global Land–Atmosphere Coupling Experiment. 2. Analysis. *Journal of Hydrometeorology,* **7**, 612-625.

Hirabayashi, Y., Kanae, S., Struthers, I. and Oki, T., 2005. A 100-year (1901-2000) global retrospective estimation of the terrestrial water cycle. *Journal of Geophysical Res*earch, **110**(D19), D19101, doi:10.1029/2004JD005492.

Hourdin, F. and co-authors, 2010. AMMA-Model Intercomparison project, *Bulletin of American Meteorological Society, January 2010*, 1-10.

Kanae, S., Oki. T. and Musiake K., 2001. Impact of deforestation on regional precipitation over the Indochina peninsula, *Journal of Hydrometeor*ology, **2**, 51-70.

Kanae, S., Hirabayashi, Y., Yamada, T. and Oki, T., 2006. Influence of "Realistic" Land Surface Wetness on Predictability of Seasonal Precipitation in Boral Summer. *Journal of Climate*, **19**, 1450-1460.

Koster, R. D., Suarez, M. J. and Heiser, M., 2000. Variance and predictability of precipitation at seasonal-to-interannual timescales. *Journal of Hydrometeorology*, **1**, 26-46.

Koster, R. D. and Suarez, M. J., 2001. Soil Moisture Memory in Climate Models. *Journal of Hydrometeorology*, **2**, 558-570.

Koster, R. D., Dirmeyer, P. A., Hahmann, A. N., Ipelaar, R., Tyahla, L., Cox, P. and Suarez, M. J., 2002. Comparing the degree of land–atmosphere interaction in four atmospheric general circulation models. *Journal of Hydrometeor*ology, **3**, 363–375.

Koster, R. D. and 24 co-authors., 2004. Regions of coupling between soil moisture and precipitation. *Science*, **305**, 1138–1140.

Koster, R. D. and 24 co-authors, 2006. GLACE: The Global Land–Atmosphere Coupling Experiment. 1. Overview and results. *Journal of Hydrometeorology*, **7**, 590-610.

Koster, R. D. and 22 co-authors, 2010. Contribution of land surface initialization to subseasonal forecast skill, First results from a multi-model experiment. Geophysical Research Letters, **37**, L02402, doi:10.1029/2009GL041677.

Mellor, G. L. and Yamada. T., 1982. Development of a turbulence closure model for geostrophic fluid problems. *Reviews of Geophysics*, **20**, 851-875.

Numaguti, A., Takahashi, M., Nakajima, T. and Sumi, A., 1997. Description of CCSR/NIES atmospheric general circulation model. *CGER's Supercomputer Monograph Report*, **3**, NIES, Tsukuba, Japan, pp. 1–48.

Onogi, T. and co-authors., 2007. The JRA-25 Reanalysis. *Journal of the Meteorological Society of Japan*, **85**, 369-432.

Reichle, R. H., Crow, W. T., Koster, R. D., Sharif, H. and Mahanama, S. P., 2008. Contribution of soil moisture retrievals to land data assimilation products, *Geophysical Research Letters*, **35**, L01404, doi: 10.1029/2007GL031986.

Seneviratne, S. I. and 10 co-authors, 2006. Soil moisture memory in AGCM simulations, analysis of global land-atmosphere coupling experiment (GLACE) data. *Journal of Hydrometeorology*, **7**, 1090-1111.

Shinoda, M. and Yamaguchi, Y., 2003. Influence of Soil Moisture Anomaly on Temperature in the Sahel: A Comparison between Wet and Dry Decades, *Journal of Hydrometeorology*, **4**, 437-447.

Shukla, J. and Mintz, Y., 1982. Influence of land-surface evapotranspiration on the Earth's climate. *Science*, **215**, 1498-1501.

Sultan, B., Janicot, S. and Diedhiou, A., 2003. The West African monsoon dynamics. Part II: the "preonset" and "onset" of the summer monsoon. *Journal of Climate*, **16**, 3389-3406.

Takata, K., Emori, S. and Watanabe, T., 2003. Development of the Minimal Advanced Treatments of Surface Interaction and Runoff (MATSIRO). *Global Planetary Change*, 209–222.

Van Den Hurk, B. J. J. M. and Van Meijgaard, E., 2010. Diagnosing Land-Atmosphere Interaction from a Regional Climate Model Simulation over West Africa. *Journal of Hydrometeorology*, **11**, 467-481.

Van Der Ent, R. J., Savenije, H. G., B. Schaefli, and Steele-Dunne, S. C., 2010. Origin and fate of atmospheric moisture over continents. *Water Resource Research*, **46**, doi:10.1029/2010WR009127.

Vinnikov, K. Y. and Yeserkepova, I. B., 1991. Soil moisture, empirical data and model results. *Journal of Climate*, **4**, 66-79.

Vizy, E. K. and Cook, K. H., 2000. Mechanisms by Which Gulf of Guinea and Eastern North Atlantic Sea Surface Temperature Anomalies Can Influence African Rainfall. *Journal of Climate*, **14**, 795-821.

Vizy, E. K. and Cook, K. H., 2002. Development and application of a mesoscale climate model for the tropics: Influence of sea surface temperature anomalies on the West African monsoon. *Journal of Geophysical Research*, **107**, 10.1029/2001JD000686.

Webster, P. J., Palmer, T. N., Yanai, M., Shukla, J., Magnana, V. and Yasunari, T., 1998. The monsoon: Processes, predictability and prediction. *Journal of Geophysical Research*, **103**, 14 451-14 510.

Xue, Y. and co-authors., 2010. Intercomparison and analyses of the climatology of the West African Monsoon in the West African Monson Modeling and Evaluation project (WAMME) first model intercomparison experiment, *Climate Dynamics*, DOI 10.1007/s00382-010-0778-2.

Yamada, T. J., Koster, R. D., Kanae, S. and Oki, T., 2007. Estimation of predictability with a newly derived index to quantify similarity among ensemble members. *Monthly Weather Rev*iew, **135**, 2674-2684.

Yamada T. J., Kanae, S., Oki, T., and Hirabayashi, Y., 2012. The onset of the West African monsoon simulated in a high-resolution atmospheric general circulation model with reanalyzed soil moisture fields. *Atmospheric Science Letters*, DOI: 10.1002/asl.367.

Figure 1: Seasonal averaged precipitation and horizontal wind vectors at 850hPa level. GSWP2 dataset is used for precipitation and wind vectors are calculated by JRA-25

Figure 2: Seasonal averaged precipitation and horizontal wind vectors at 850hPa level in the ensemble mean of W Experiment.

Figure 3: Global distributions of $\Omega_P(R)-\Omega_P(W)$ in 4 seasons. (a): MAM; (b): JJA; (c): SON; (d): DJF. 0.06 is 95% statistical significance level.

Figure 4: Time series of Ω_P index for W (blue line) and R (red line) experiments over the western Sahel (10°N-15°E; 0-10°E). Both lines are calculated by 15-day moving average window. (b) Time series of $\sigma_E(W)\left[\Omega_E(R)-\Omega_E(W)\right]$ over the same region.

Figure 5: 6day-averaged time series of precipitation (mm/day) averaged in the western Sahel for W (a) and R (b) experiments. Thick lines denote ensemble mean for each experiment.

Figure 6: 6day-averaged time series of surface soil wetness averaged in the western Sahel for

(a) W experiment. (b) Scatter diagram of 6-day averaged soil wetness among 16 ensemble members in W experiment for 7 months (April to October). Each month has 5 time periods.

Figure 7: 6 day-averaged time series of cumulus cloud (blue) / large scale condensation (green) type precipitation (mm/day), and the bulk Richardson number at 925hPa height in the western Sahel. Precipitation is averaged among 16 ensemble members in W experiment.

Figure 8: 6 day-averaged time series of lifted condensation level averaged in the western Sahel both for W (a) and R (b) experiments.

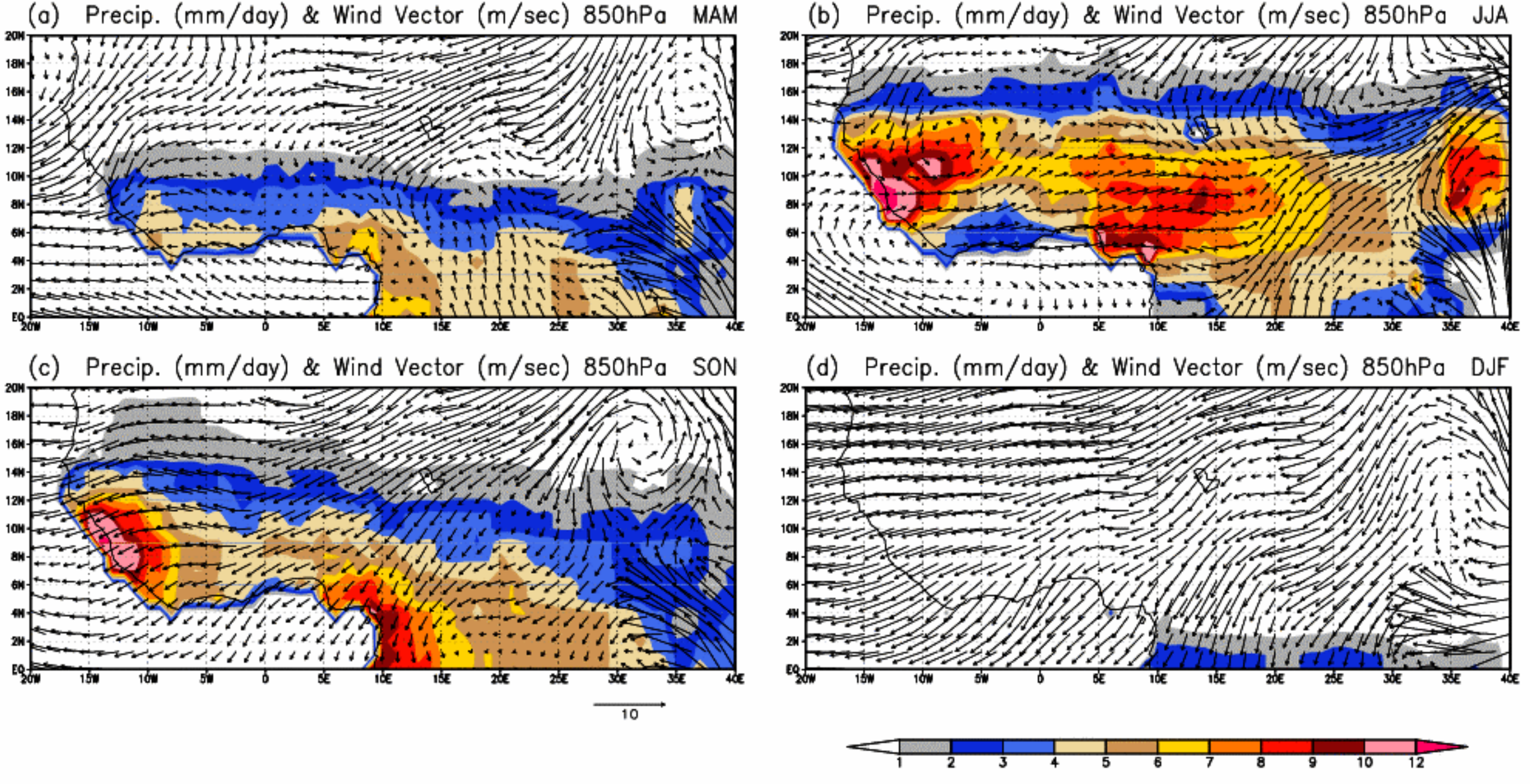
(a) Precip. (mm/day) & Wind Vector (m/sec) 850hPa MAM
(b) Precip. (mm/day) & Wind Vector (m/sec) 850hPa JJA
(c) Precip. (mm/day) & Wind Vector (m/sec) 850hPa SON
(d) Precip. (mm/day) & Wind Vector (m/sec) 850hPa DJF
20N
18N
16N
14N
12N
10N
8N
6N
4N
2N
EQ
20W
15W
10W
5W
0
5E
10E
15E
20E
25E
30E
35E
40E
10
1
2
3
4
5
6
7
8
9
10
12

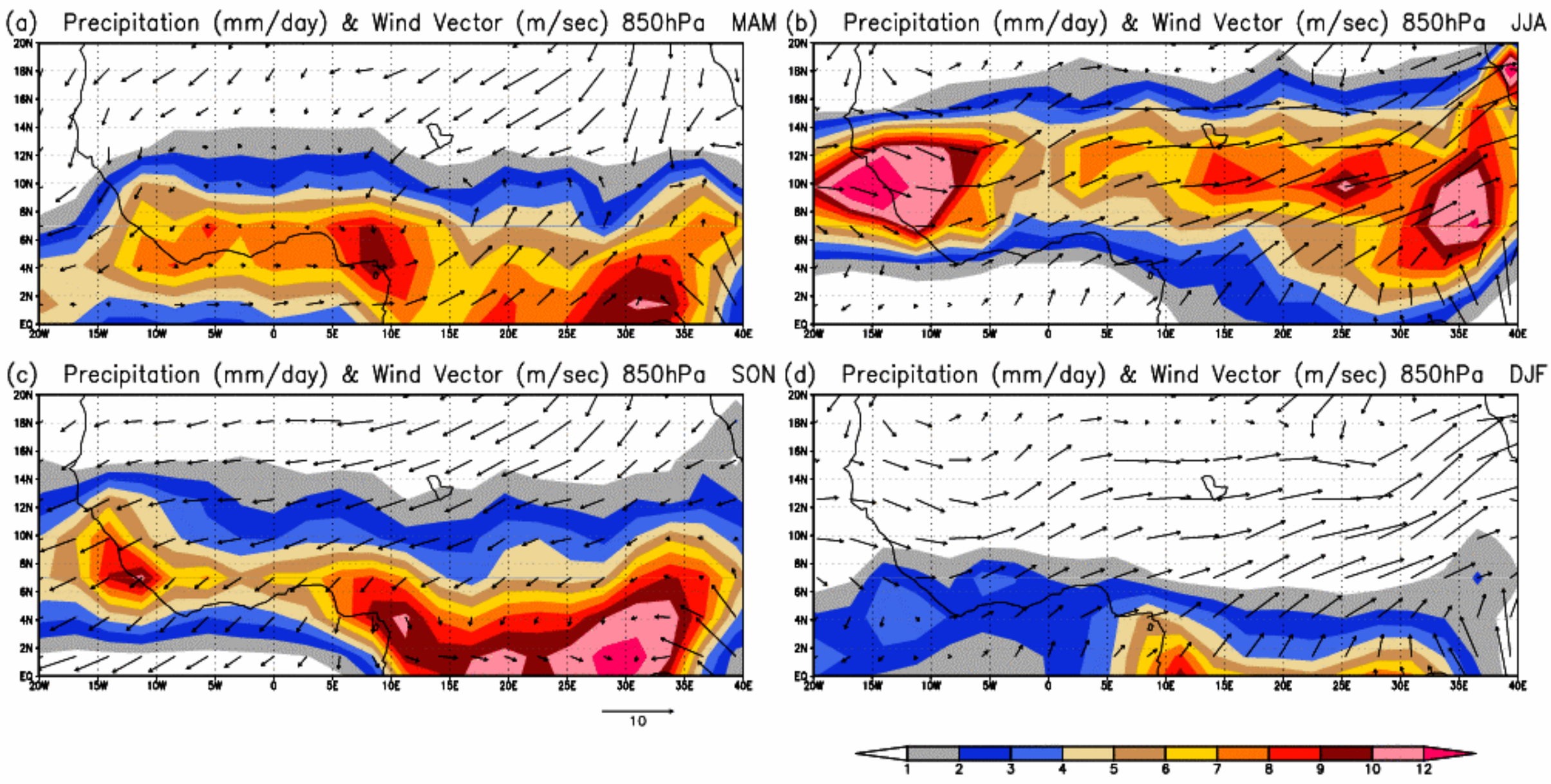
(a) Precipitation (mm/day) & Wind Vector (m/sec) 850hPa MAM
(b) Precipitation (mm/day) & Wind Vector (m/sec) 850hPa JJA
(c) Precipitation (mm/day) & Wind Vector (m/sec) 850hPa SON
(d) Precipitation (mm/day) & Wind Vector (m/sec) 850hPa DJF
20N
18N
16N
14N
12N
10N
8N
6N
4N
2N
EQ
20W
15W
10W
5W
0
5E
10E
15E
20E
25E
30E
35E
40E
10
1
2
3
4
5
6
7
8
9
10
12

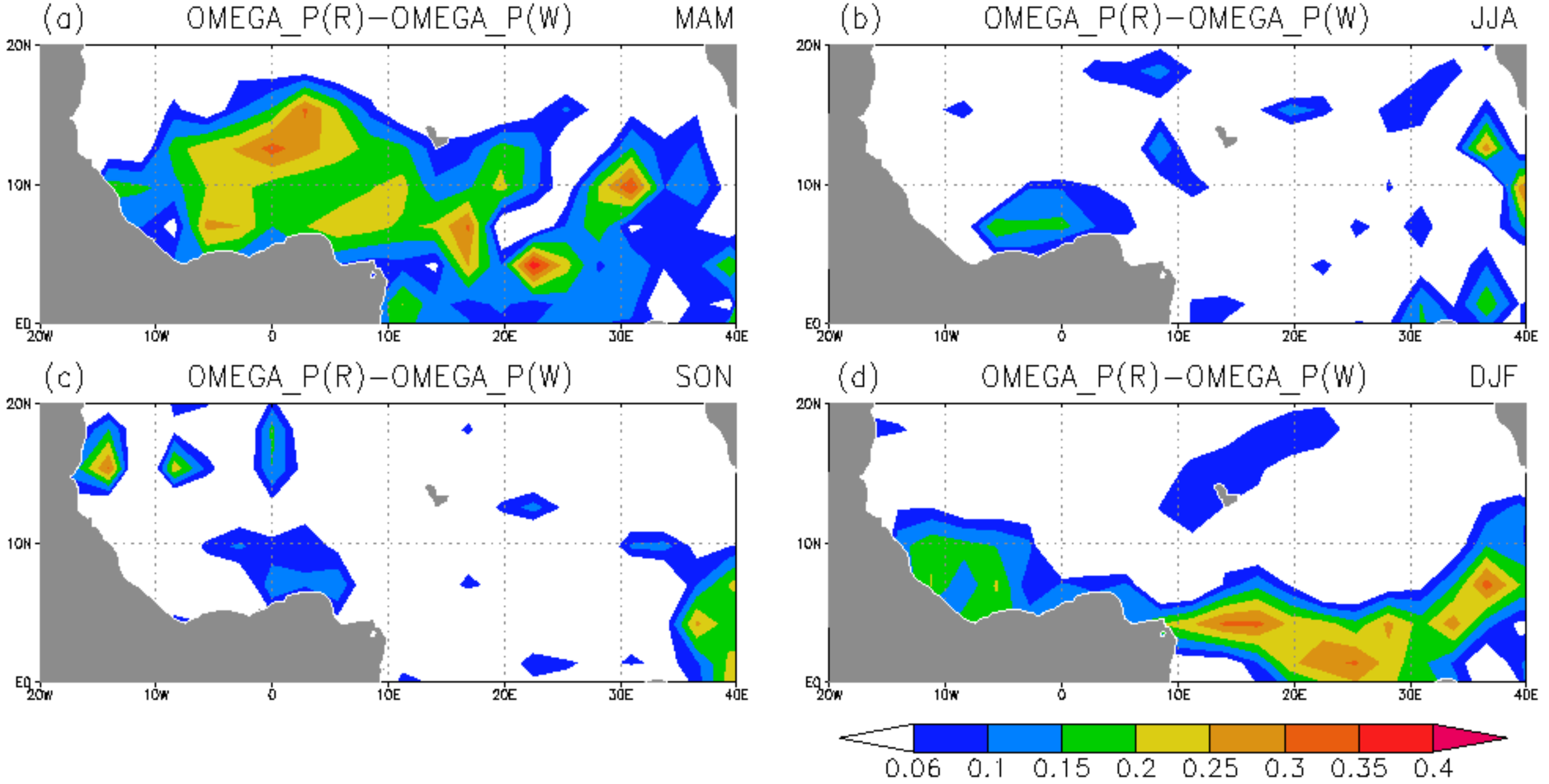
(a) OMEGA_P(R)−OMEGA_P(W) MAM
(b) OMEGA_P(R)−OMEGA_P(W) JJA
(c) OMEGA_P(R)−OMEGA_P(W) SON
(d) OMEGA_P(R)−OMEGA_P(W) DJF
20N
10N
EQ
20W
10W
0
10E
20E
30E
40E
0.06 0.1 0.15 0.2 0.25 0.3 0.35 0.4

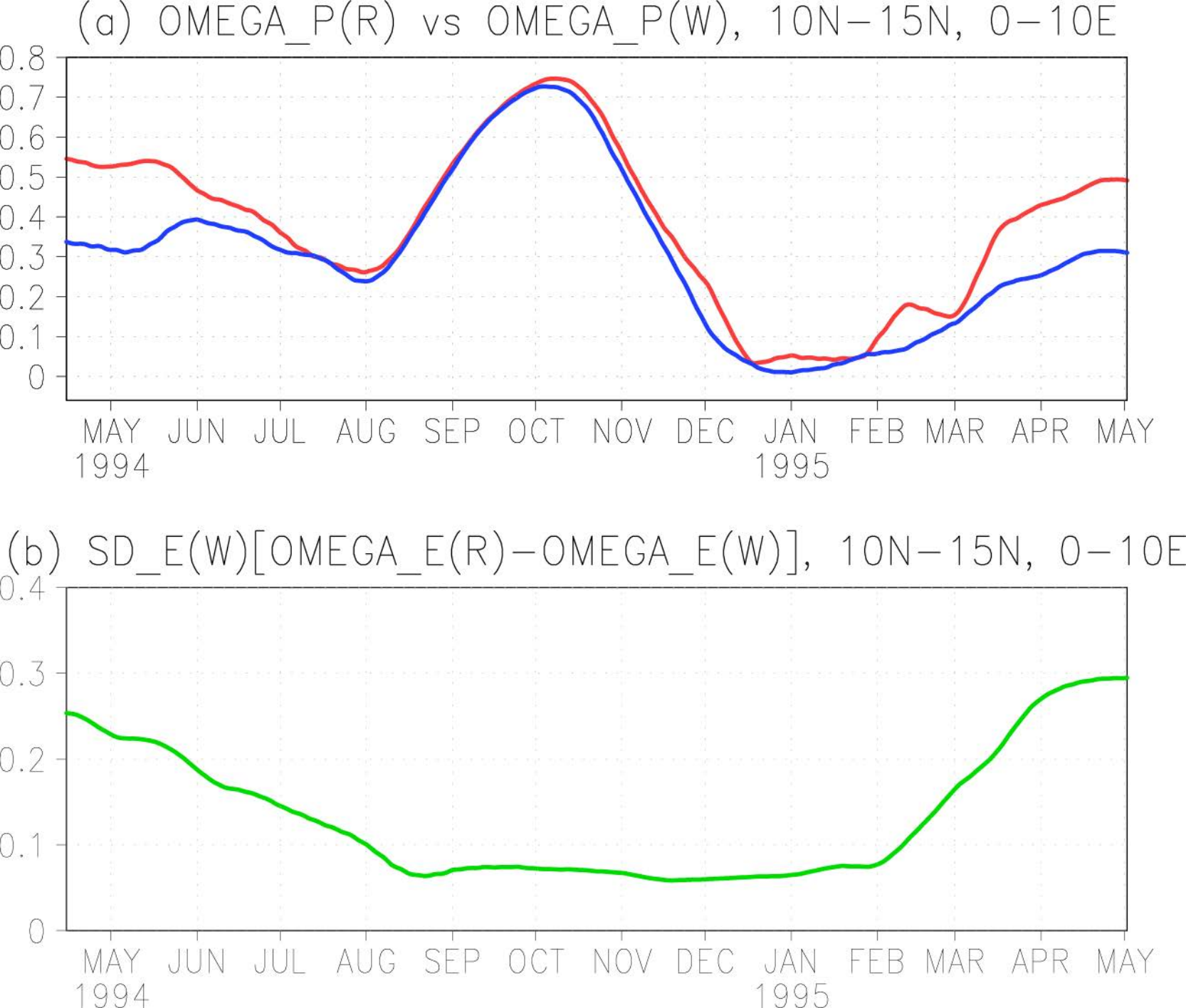
(a) OMEGA_P(R) vs OMEGA_P(W), 10N–15N, 0–10E
0.8
0.7
0.6
0.5
0.4
0.3
0.2
0.1
0
MAY JUN JUL AUG SEP OCT NOV DEC JAN FEB MAR APR MAY
1994
1995
(b) SD_E(W)[OMEGA_E(R)–OMEGA_E(W)], 10N–15N, 0–10E
0.4
0.3
0.2
0.1
0
MAY JUN JUL AUG SEP OCT NOV DEC JAN FEB MAR APR MAY
1994
1995

(a) Precip,6day−aver.,10N−15N,0−10E,W−Exp.

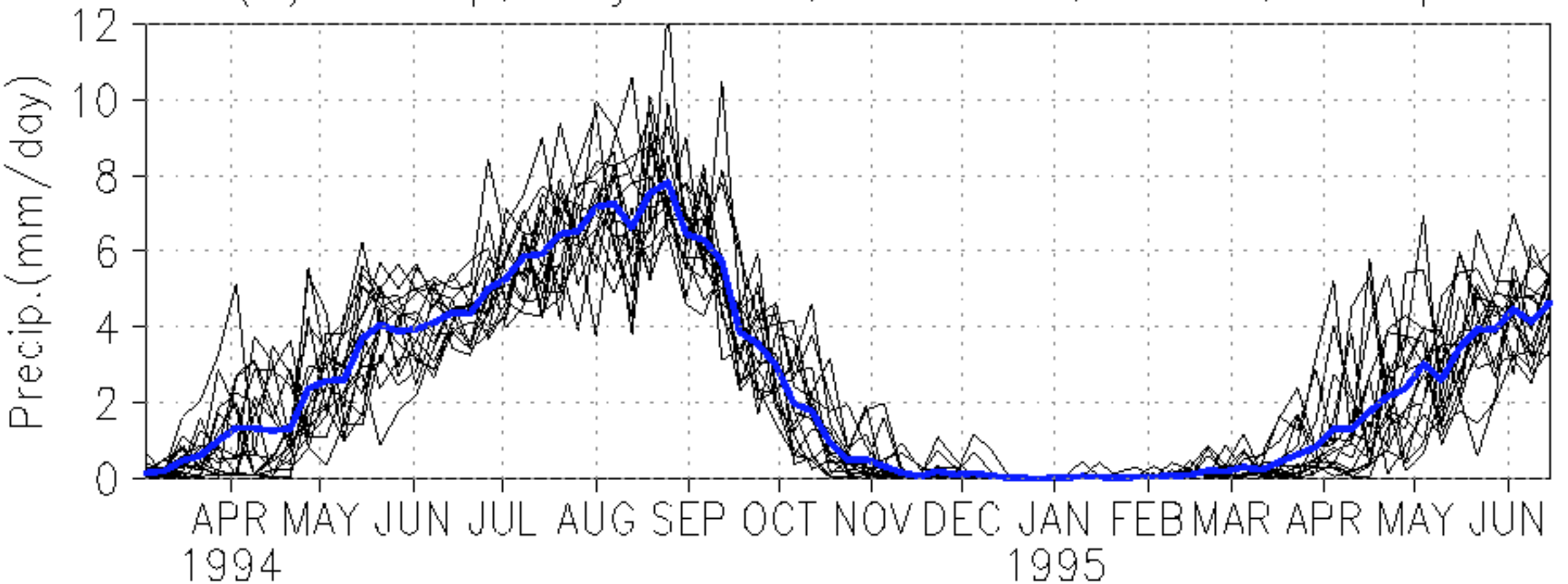

(b) Precip,6day−aver.,10N−15N,0−10E,R−Exp.

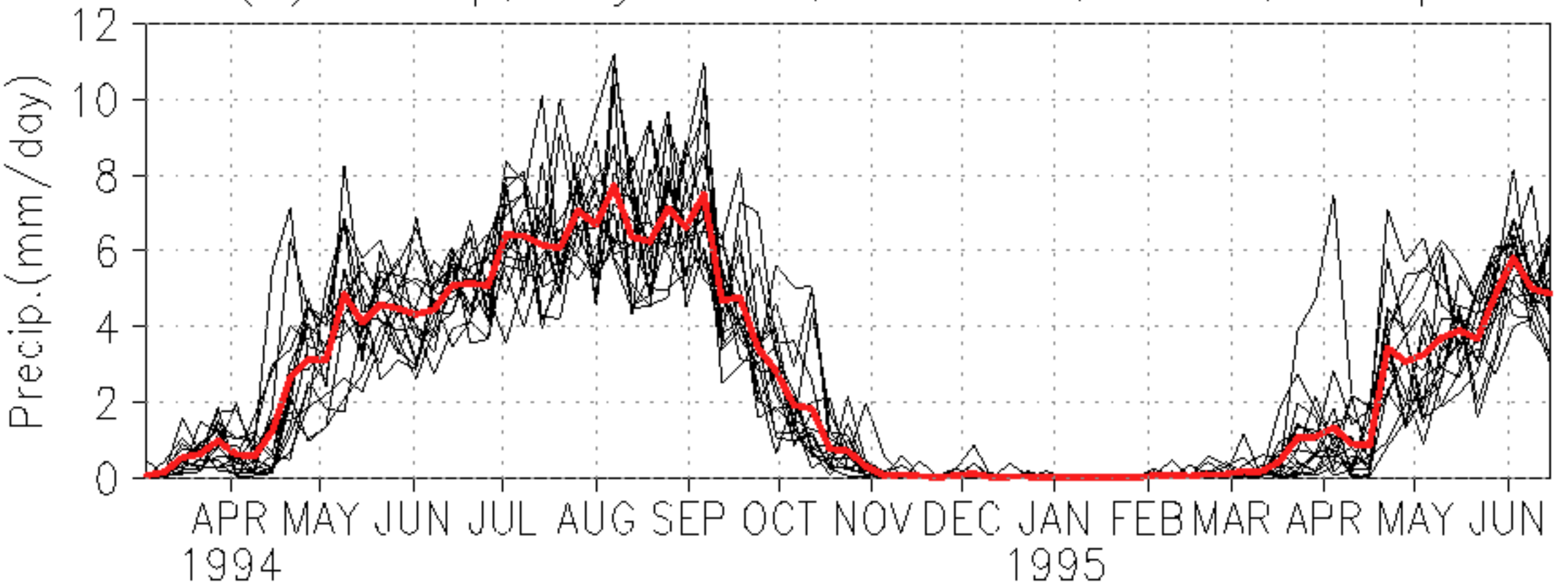

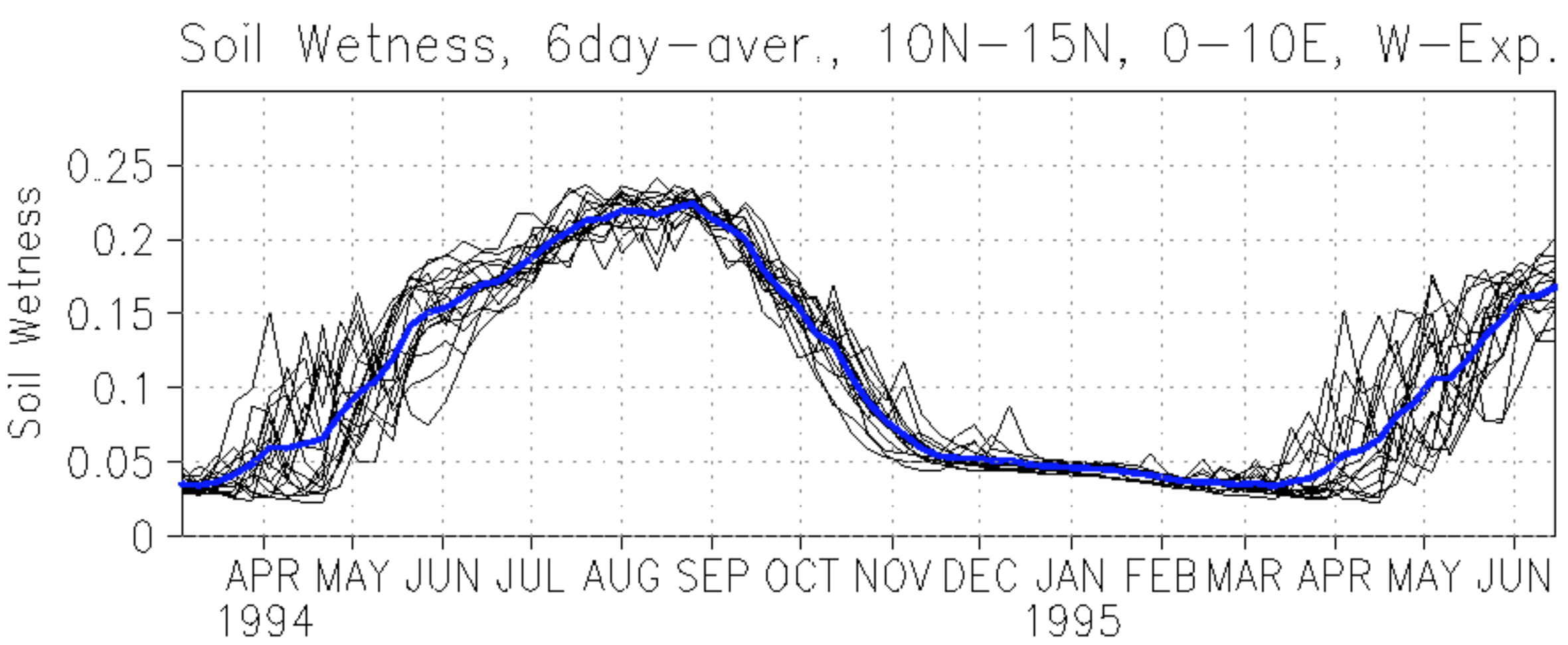
Soil Wetness, 6day-aver., 10N-15N, 0-10E, W-Exp.
Soil Wetness
0.25
0.2
0.15
0.1
0.05
0
APR MAY JUN JUL AUG SEP OCT NOV DEC JAN FEB MAR APR MAY JUN
1994
1995

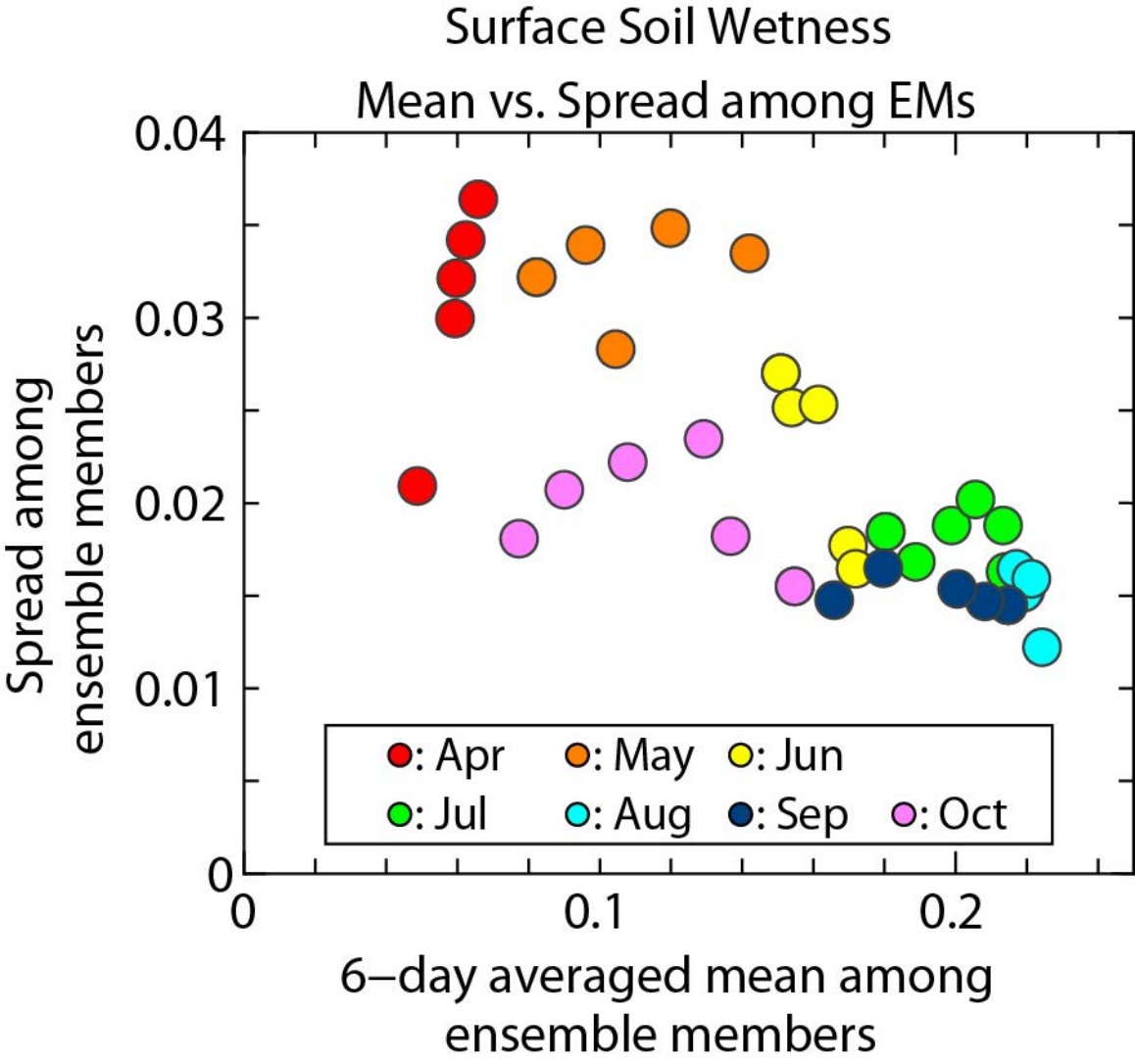
Surface Soil Wetness
Mean vs. Spread among EMs
Spread among ensemble members
6–day averaged mean among ensemble members
0.04
0.03
0.02
0.01
0
0
0.1
0.2
: Apr
: May
: Jun
: Jul
: Aug
: Sep
: Oct

(a) Precip.(mm/day),6day−aver.,10N−15N,0−10E

Precip.(mm/day)

10
8
6
4
2
0

APR MAY JUN JUL AUG SEP OCT NOV DEC JAN FEB MAR APR MAY JUN
1994 1995

(b) Bulk Richard.num.,6day−aver.,10N−15S,0−10E

Stability

0
−2
−4
−6
−8
−10
−12
−14

APR MAY JUN JUL AUG SEP OCT NOV DEC JAN FEB MAR APR MAY JUN
1994 1995

(a) LCL(hPa), 6day−aver., 10N−15N, 0−10E, W−Exp.

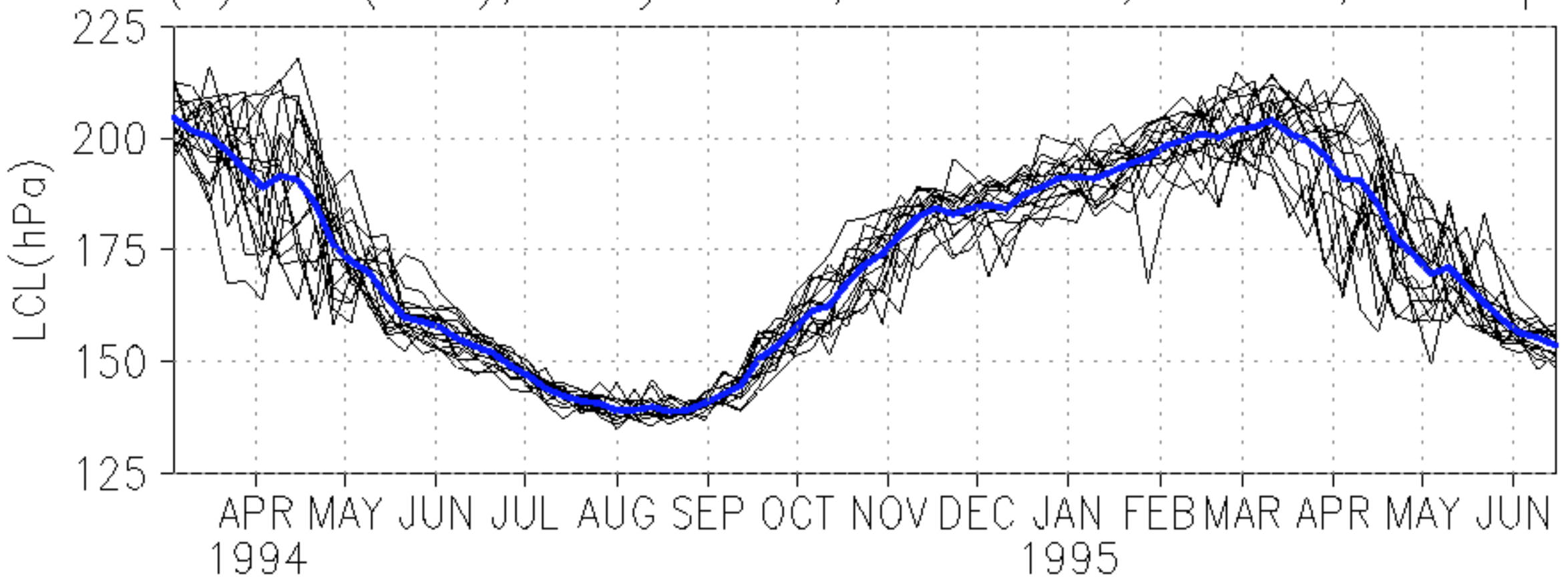

(b) LCL(hPa), 6day−aver., 10N−15N, 0−10E, R−Exp.